Continental Shelf Research 220 (2021) 104404

Contents lists available at ScienceDirect

Continental Shelf Research

journal homepage: http://www.elsevier.com/locate/csr

Volcanism and rapid sedimentation affect the benthic communities of Deception Island, Antarctica

Carlos Angulo-Preckler [a,b,*], Philippe Pernet [c], Cristina García-Hernández [d], Gabor Kereszturi [e], Antonio M. Álvarez-Valero [f], Joaquín Hopfenblatt [g], María Gómez-Ballesteros [h], Xosé L. Otero [i], Jaime Caza [i], Jesús Ruiz-Fernández [d], Adelina Geyer [g], Conxita Avila [a]

[a] University of Barcelona and IRBio (Research Institute of Biodiversity), Barcelona, Catalonia, Spain
[b] Norwegian College of Fishery Science. UiT The Arctic University of Norway, Tromsø, Norway
[c] Laboratorie de Biologie Marine, Université Libre de Bruxelles, Belgium
[d] Department of Geography. University of Oviedo, Spain
[e] Volcanic Risk Solutions, School of Agriculture and Environment, Massey University, Palmerston North, 4474, New Zealand
[f] Department of Geology. University of Salamanca. Faculty of Sciences, 37008, Salamanca, Spain
[g] Geosciences Barcelona, Geo3Bcn, CSIC, Lluis Sole i Sabaris s/n, 08028, Barcelona, Spain
[h] Spanish Oceanographic Institute (IEO), Madrid, Spain
[i] CRETUS Institute. Department of Edaphology and Agricultural Chemistry. University of Santiago de Compostela, Spain

ARTICLE INFO

Keywords:
Marine macroinvertebrates
Submarine volcano
Geochemistry
Petrology
Biodiversity
South Shetland islands

ABSTRACT

Deception Island is amongst the most active volcanoes in the Southern Ocean, with over 20 explosive eruptions in the last ca. 200 years. The eruption that formed the caldera at Deception Island occurred 3980 ± 125 calendar years Before Present, and it is the largest eruptive event documented in Antarctica during Holocene. Since then, post-caldera volcanic activity has comprised many scattered eruptive vents across the island. Mortality of benthic organisms has been reported during the most recent eruptions occurred on the island, in 1967, 1969, and 1970 Common Era (CE), with very low abundances of organisms during the 1967–1973 CE period. Within the sea-flooded part of the caldera depression, named Port Foster, a submarine volcanic axis with several volcanic cones is observed. An interdisciplinary team sampled the best morphologically preserved volcanic edifice within Port Foster, the so-called Stanley Patch. Geophysical data traced the volcano and characterized its morphology and inner structure. Underwater scuba sampling allowed to acquire sediment and rock samples, photographs and video images of the benthic organisms and seascape. Morphology of Stanley Patch cone and textural characteristics of the collected pyroclastic rocks indicate that the volcanic edifice was originated during an explosive eruption. Furthermore, the lack of palagonitization, quenched pyroclast margins, and hyaloclastite deposits indicate that this cone has formed on-land, before the caldera floor became inundated by the seawater, highlighting the complex intra-caldera evolution of Deception Island. A sediment core from the crater was collected for sedimentological, and geochemical analysis. Antarctic climate and seasonal sea ice, together with organic degradation due to high sedimentation rates, explain the low total organic carbon data measured. The volcanic history of the island has probably avoided the development of a stable benthic community over time, similar to other Antarctic shallow communities. Moreover, the current geomorphological conditions still shape different benthic communities than in the surrounding coastal ecosystems. Stanley Patch, and the whole Port Foster, provide a natural laboratory for benchmarking the reestablishment of benthic communities on a volcanic-influenced shallow marine environment, offering relevant data for future studies evaluating global climate change effects on the Antarctic seabed.

* Corresponding author.
E-mail address: carlos.a.preckler@uit.no (C. Angulo-Preckler).

https://doi.org/10.1016/j.csr.2021.104404
Received 16 April 2020; Received in revised form 24 February 2021; Accepted 8 March 2021
Available online 17 March 2021

1. Introduction

Antarctic volcanoes are extremely active and have produced multiple volcanic eruptions in historical times (LeMasurier and Thomson 1990). Deception Island, located in the South Shetland Islands, is amongst the most active volcanoes in the Southern Ocean, with a record of over 20 explosive eruptions in the last two centuries (e.g. Orheim et al., 1972; Roobol, 1982; Smellie et al., 2002). Indeed, the eruption record from the eighteenth to the twentieth centuries comprises periods of high activity (e.g. 1818–1828 CE, 1906–1912 CE, 1967–1970 CE) with numerous eruptions closely spaced in time, followed by decades of dormancy (e.g. 1912–1967 CE) (Orheim 1972; Roobol 1980, 1982; Smellie 2002).

Periodic disturbance is a key factor in most ecosystems and is a selective force influencing species composition and assemblage structure (Dell et al., 2019; Robinson et al., 2020). While in shallow coastal areas of Antarctica, the benthic communities are mainly influenced by ice disturbance (Smale 2008), in Deception Island, factors such as volcanic activity and sedimentation may impose the distribution and abundance of macroinvertebrates (Brierley, 1999; Barnes et al., 2008). However, there is still a lack of knowledge on how natural disturbance processes with such disparate time scales can be influencing the composition and structure of current communities on a small spatial scale. Thus, it is important to understand the underlying mechanisms linking species composition, disturbance, and other drivers of assemblage structure.

During January 2018, a multidisciplinary team worked together to

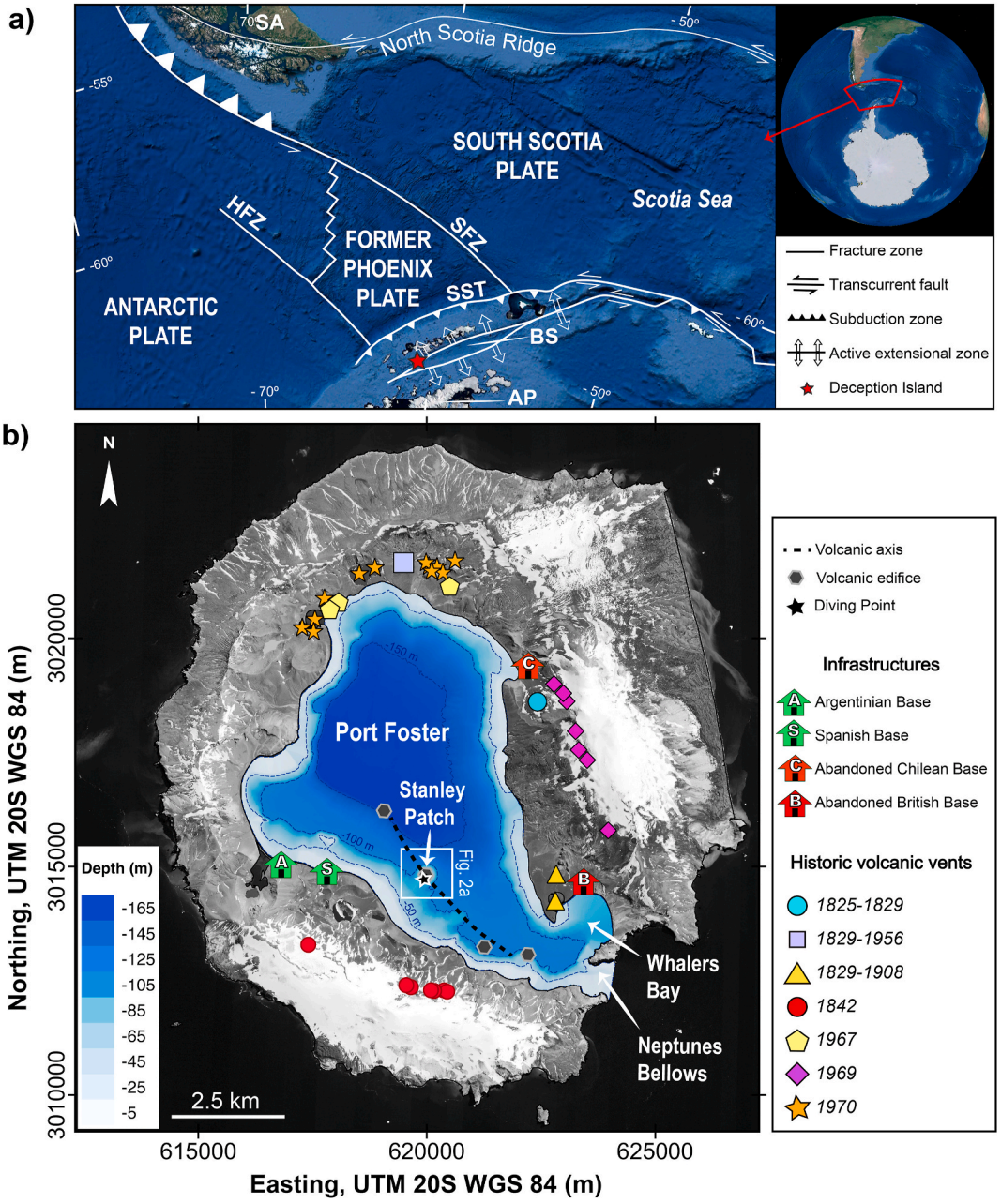

Fig. 1. **(a)** Simplified regional tectonic map and location of the South Shetland Islands (modified from Martos et al., 2014). AP: Antarctic Peninsula, BS: Bransfield Strait, HFZ Hero Fracture Zone, SFZ Shetland Fracture Zone, SST: South Shetland Trench. Google Earth image source: Landsat/Copernicus – U.S. Geological Survey **(b)** Deception Island orthophotomap (data obtained from Spatial Data Infrastructure for Deception Island SIMAC, Torrecillas et al., 2006) where active and abandoned scientific stations, as well as historic volcanic vents (data from Roobol, 1973, 1980, 1982; Baker et al., 1975, Smellie, 2002b; Baker and McReath, 1971) and submarine volcanic edifices along volcanic axis (Rey et al., 1995) are indicated.

sample Stanley Patch for the first time. Stanley Patch is the largest and best morphologically preserved volcanic cone inside Port Foster. The study allows for an integrative understanding of this volcanic system from environmental, ecological, and volcanological perspectives. We also highlight the importance of multidisciplinary studies to advance in the general understanding of the bio-geological knowledge of submarine volcanic terrains, and at Deception Island in particular.

1.1. Site description

Deception Island is located at the southwestern end of the Bransfield Strait, an actively extending young (probably <4 My old; Barker, 1982) marginal basin between the Antarctic Peninsula and South Shetland Islands. The volcanic and magmatic evolution of the island is marked by a large eruption that occurred 3980 ± 125 calibrated years Before Present (BP) (Antoniades et al., 2018). This event led to the catastrophic collapse and sinking of the major volcanic edifice that generated the current caldera (Rey et al., 1995; Smellie, 2002). Port Foster bay, which opens onto the sea through the narrow strait of Neptunes Bellows, occupies the central part of the island and corresponds to the sea-flooded part of the caldera depression. Volcanic activity occurring after the caldera-forming event, which includes the recent historical eruptions (Fig. 1), comprises several tens of scattered eruptive vents across the whole island (e.g., Smellie et al., 2002; Martí et al., 2013). Within Port Foster, a submarine volcanic axis composed of several volcanic cones can be distinguished (Rey et al., 1995; Somoza et al., 2004). Some of these volcanic edifices, mainly located at the southern part of the bay, are morphologically well-preserved and rise up to more than 50 m from the seafloor.

Port Foster constitutes a closed natural sedimentary basin, with lateral contributions of terrigenous, fine volcanogenic sediments of fluvioglacial, periglacial, aeolian and marine origin with biodetritic components (Baldwin and Smith, 2003). The coastal and submarine deposits are regulated by processes related to the steep slopes covered by glaciers surrounding the caldera (López-Martínez et al., 1999). The interaction of volcanic material and ice results in the establishment of active torrential streams during the austral summer that carry sediment to the basin. Long-term volcanic tremors also promote avalanches of sedimentary fillings on the steep slopes (Rey et al., 1992). The submarine morphologies and the depositional characteristics of Port Foster suggest a strong tectonic control over the submarine geomorphology, which affects the intensity of the fluvioglacial processes. The sediment particulate flux in Port Foster is considerably higher than that in the nearby Bransfield Strait, with winter fluxes up to five orders of magnitude larger (Baldwin and Smith, 2003).

The composition of the seafloor communities is the product of numerous biological and physical processes acting across multiple spatial and temporal scales (Pickett and Kolasa, 1991). Significant inputs of freshwater, sediments, and associated minerals are observed in areas in proximity to ice shelves and glaciers, and the associated runoff with melting (Pasotti et al., 2015; Dayton et al., 2016; Monien et al., 2017). Nearshore communities, often rich in primary production, are at the boundary between terrestrial and open ocean systems. The volcanic eruptions of 1967, 1969, and 1970 CE, led to a complete mortality of local marine benthic organisms (Gallardo and Castillo 1968; Gallardo et al., 1977). These communities suffered an enormous impact that lasted several years, when the abundance of macroorganisms was reported to be very low from 1967 to 1973 CE (Lovell and Trego, 2003). Shallow benthic communities inside Port Foster have since apparently recovered, with a dominance of vagile invertebrates, particularly echinoderms such as brittle stars, sea stars, and sea urchins (Cranmer et al., 2003; Angulo-Preckler et al., 2017b). Furthermore, an important community of suspension-feeders (mainly sponges, bryozoans, and ascidians) are found in the scarce hard bottoms described within Port Foster (Angulo-Preckler et al., 2018). Also, bivalves contribute to the suspension feeding communities stablished in the soft-bottoms at Deception Island (Angulo-Preckler et al., 2018).

2. Material & methods

Fieldwork during the 2017–2018 Antarctic season targeted the shallowest point of Stanley Patch, the cone summit at the southern side of the crater rim located at 25 m depth below sea level. The objective was to access and observe the general submarine scenario, to identify the macrobenthic communities living on it, as well as to collect both a sediment core and rock samples by SCUBA diving. To complete the study, the divers took underwater photographs and videos. Selected invertebrates were collected to identify the species forming the benthic community that inhabits the volcano. Samples for sedimentological analysis provide information about the environmental evolution since the cone formation and a minimum age for the volcano based on radiocarbon dating. Furthermore, the morphology of Stanley Patch volcano has been mapped in detail using the bathymetry data (IHM, 2018) collected in the bay, aboard the R.V. BIO-Hesperides, by the Instituto Español de Oceanografía (IEO) and Instituto Hidrográfico de la Marina (IHM). Bathymetric data was obtained with a multibeam echosounder system, including a Kongsberg EM-12, operating 191 beams at a 12 kHz frequency and a GeoSwath system in the shallowest areas. From these data, a 9 × 9 m resolution digital elevation model (DEM) of Stanley Patch volcano (Fig. 2a and b) was constructed with Caris Hips & Sips software.

Volcanology and Petrology. Twenty-one rock samples of 3–15 cm in diameter size were collected at the southern side of the crater rim. A subset of three less weathered representative samples were selected for the sedimentological, petrographic, and geochemical descriptions. Thin sections were prepared and whole rock major and trace elements were analyzed for each sample using x-ray fluorescence (XRF) and inductively coupled plasma - mass spectrometry (ICP-MS), respectively. For XRF analysis a ThermoARL Advant'XP + sequential X-ray spectrometer was used at the GeoAnalytical Lab at Washington State University (WSU) (https://environment.wsu.edu/facilities/geoanalytical-lab/technical-notes/xrf-method/). Loss on ignition (LOI) as a proxy for volatile content was measured using standard thermogravimetric methods at WSU. Trace elements and rare Earth elements (REE) were also analyzed for the same samples by ICP-MS using an Agilent 7700 at WSU (https://environment.wsu.edu/facilities/geoanalytical-lab/technical-notes/icp-ms-method/). Relative precision was in general better than 1% (RSD) for major oxides and trace elements, under 5% for REE, and under 10% for the remaining trace elements.

Morphometric parameters of Stanley Patch volcanic cone were manually measured using Quantum GIS, version 3.10 A Coruña (https://www. qgis.org/en/site/). A shaded relief model was created from the DEM to delineate the extent of the crater and cone based on break-in-slopes. The morphometric parameters obtained were the following (Fig. 2c): (i) cone height (Hco) calculated as the difference between the maximum elevation of the cone rim (i.e. shallowest point below sea level) and the average basal depth of the cone (Settle, 1979); (ii) average diameter of the cone crater (Wcr) obtained from the planimetric area of the crater (Acr) as $(4*Acr/\pi)^{0.5}$ (Favalli et al., 2009); and (iii) average basal diameter of the cone (Wco) obtained from the planimetric projection of the cone basal area (Aco) as $(4*Aco/\pi)^{0.5}$.

Sedimentological and geochemical analysis. A push core from the crater rim was collected (62.98°S, 60.63°W). The sample was taken manually, and the rocky substrate was not reached. The sediment core (4 cm in diameter and 8 cm in length) was subsampled every centimetre for sedimentological and geochemical analysis. In order to minimize the oxidation of sediment material, samples were frozen at −20 °C until the physico-chemical analyses were performed. The pH and redox potential (Eh) were determined *in situ* with portable electrodes (HANNA instruments INC, Woonsocket, RI, U.S.A.). The Eh values were corrected by adding the potential of a reference electrode (+244 mV). Oxic

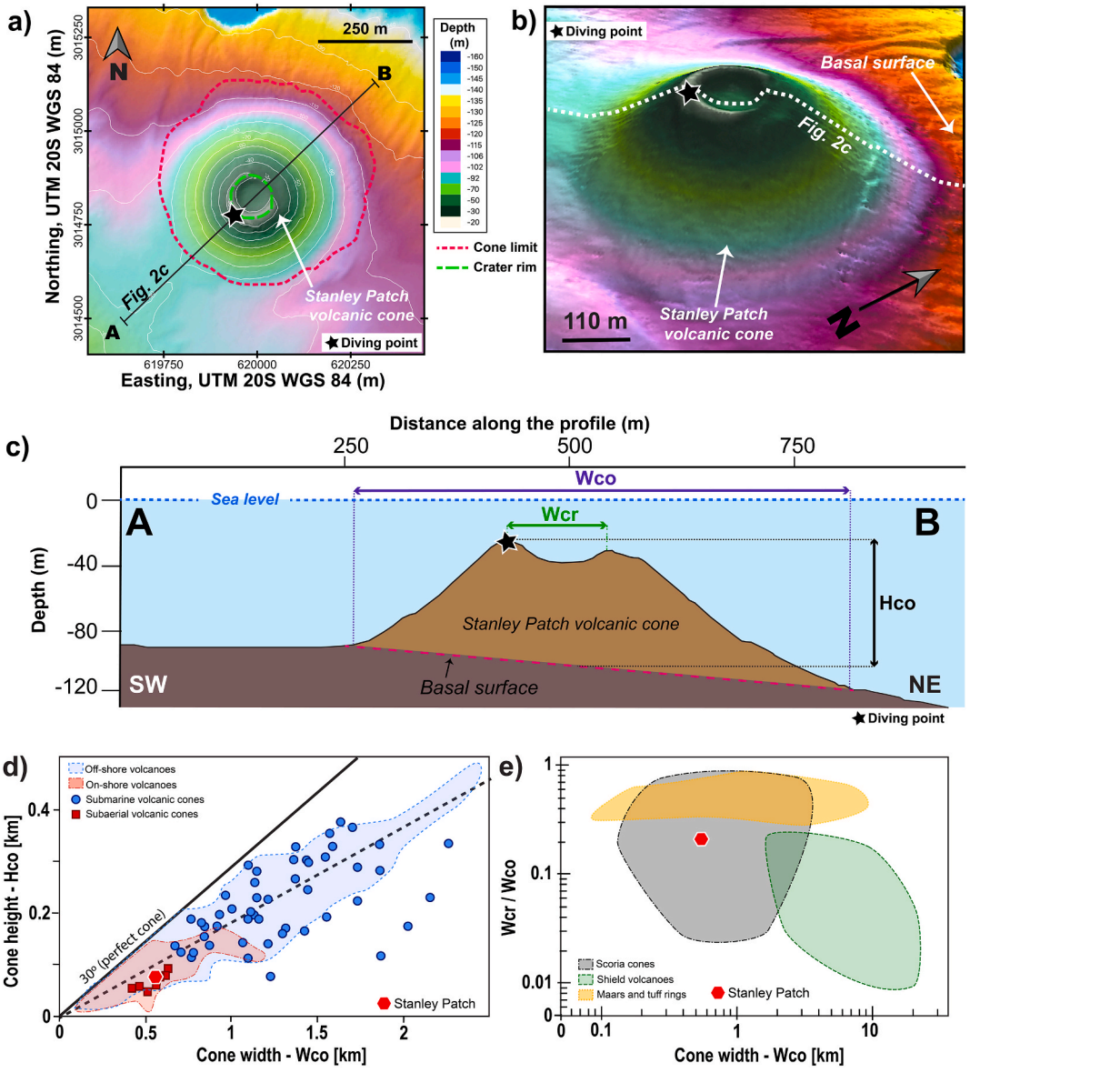

Fig. 2. Bathymetric **(a)** and 3D shaded relief map **(b)** of Stanley Patch volcano, showing the location of the profiles displayed at c). **(c)** Terrain profile crossing Stanley Patch volcano along the line A-B (see (a) for location). At the profile are marked the morphological parameters measured at the cone (Wco, Wcr, and Hco); **(d)** Average basal width (Wco) vs height (Hco) for Stanley Patch volcano compared to well-studied on-shore and off-shore volcanic edifices observed at Pico Island (Açores) (blue circles and red squares, data from Mitchell et al., 2012) and Terceira Rift/San Miguel island (blue and red area, data from Weiβ et al., 2015). **(e)** Wcr/Wco ratio vs. height Hco of Stanley Patch volcano compared to the values for several other types of terrestrial volcanic edifices according to Brož and Hauber (2013).

microsites (i.e. presence of molecular oxygen) were considered when Eh > 350 mV, suboxic (i.e. reduction of oxyhydroxides of Fe (III)/Mn(IV) when Eh = 350-100 mV, and anoxic (i.e. reduction of sulphate) when Eh > 100 mV (see Ponnamperuma, 1972; Ferreira et al., 2006). Particle sizes were separated using the Robinson pipette method (Gee and Bauder, 1986). Twenty grams of dry sample were subjected to attack by hydrogen peroxide (15%) for 72 h to remove organic matter; 50 ml HCl (1M) were then added and left for 20 min, occasionally shaking, to remove Fe and Al oxides and hydroxides. Organic substances and Fe/Al oxides were removed because they act as sediment particle aggregating components. The sample was then washed until free from chlorides, and sodium hexametaphosphate was added as a dispersing agent. Mechanical agitation (2 h) used in combination with chemical treatments enhances dispersal. After dispersal, the sand fraction (0.05–2 mm) was separated by sieving through a 0.05 mm mesh size, while particles with diameter <0.05 mm (silt and clay) were separated by sedimentation in water. During sand particle separation, the solution and particles (silt + clay) were collected in a bucket after passing through the sieve and were then transferred to a 1 L beaker. This solution was thoroughly stirred to achieve suspension of all soil particles. Immediately after stirring, 20 mL of the suspension were extracted at 10 cm depth using a Robinson pipette. This subsample contained both fractions: silt and clay. The sample was dried at 105 °C and weighed. After leaving to rest for 8 h, the silt fraction had sedimented and the clay fraction could be extracted following the same procedure. The subsample was dried at 105 °C and weighed. To calculate the amount of clay present in the total sediment sample, the amount of clay present in 20 mL was multiplied by 50 to yield the amount of clay in 1 L of suspension and, therefore, in the sediment sample. The amount of silt was calculated by subtracting the amount of clay from the subsample (silt + clay) and following the same procedure as with the clay fraction. The weight in grams was finally obtained for the sand, silt, and clay fractions. The three fractions were

added (=100%) and the % weight of the individual fractions was calculated based on the weight of each one.

The total organic carbon (TOC) and total nitrogen (TN) contents were determined in a TruSpec CHNS analyser (LECO Corp., St Joseph, MI, USA), while total sulfur (TS) were measured in an SC-144DR analyser. Prior to the TOC determination, the samples were attacked with 1M HCl at 60 °C until dry in order to eliminate the carbonates (Huerta-Díaz and Morse, 1992). Calibration was realized with different LECO standards and percentage of recovery obtained: 100.1 ± 1.3% for C, 99.7 ± 1.7% and 99.9 ± 1.3% for S (n = 4). The ratio TOC/TN was used as a proxy of organic matter origin (terrigenous organic matter C/N > 20, Emerson and Hedges, 1988).

The concentration of metastable Fe sulphides fraction (acid volatile sulphides AVS = $\sum$FeS, Fe_3S_4) was determined in duplicate using 0.5–1 g of wet sample, according to the method described by Kostka and Luther (1994). Sulphide from AVS was liberated with 20 ml 6N HCl previously deaerated for 40–50 min. The sample was digested in a gas-tight reaction flask for 40–50 min under a continuous flow of nitrogen, which was bubbled through the flask as slowly as possible. The evolved H_2S was then received in a trap containing 25 ml of 3% Zn acetate, 1 mL of concentrated H_2SO_4, and 4 mL of diamine reagent, and precipitated as ZnS. Sulphide was then measured colorimetrically with a UV-VIS spectrophotometer at a wavelength of 670 nm using the methylene blue method of Cline (1969). The concentration of Fe-AVS was calculated from the concentration of AVS-S, assuming a ratio of S:Fe of 1.1 (Kostka and Luther, 1994). The concentrations were always expressed in terms of dry weight of soil (dw), the moisture content being determined from two subsamples dried at 105 °C to constant weight. In addition, the color of the sediment samples was characterized by using the Munsell Color Chart.

Biodiversity. Underwater photographs were taken by scuba-diving. The specimens were identified to species level, when possible. Due to the difficulties of the dive operation (depth, low visibility, currents, cold waters), the bottom time was limited to 15 min, and only one video transect was recorded. The distance of the transect was 50 m long. All organisms detected on half meter at each side of the central line of the video transect were counted to measure the abundance for each macrobenthic species. The density of benthic organisms was ranked in three different groups, 1) **low abundance**; species present at least one time in the transect but lower than 5 organisms per m^2, 2) **medium abundance**; between 5 and 50 organisms per m^2, and 3) **high abundance**; species with densities higher than 50 organisms per m^2.

3. Results

Volcanology and Petrology. Stanley Patch rises sharply from the north-east trending and gently dipping (~3°) seafloor at 90–120 m water depth (Fig. 2a, b and c). The edifice has a height (Hco) of 80 m and a basal diameter of ~553 m (Wco) (Fig. 2c). The crater (Wcr) has a circular shape and a diameter of 113 m. This results in an average Hco/Wco ratio of ~0.15 (Fig. 2d) and Wcr/Wco of ~0.2 (Fig. 2e). The cone has relatively uniform slope angle values of 20–30°. The morphology of the cone is well defined and hardly affected by underwater erosion (e.g. turbidites).

Based on the macroscopic observations, the Stanley Patch volcanic samples are mostly low-density scoriaceous fragments (Fig. 3, Appendix A). They display aphyric textures with phenocryst and microphenocryst contents below 1–2%. Plagioclase and minor clinopyroxene and olivine phenocrysts are set in a brown to black groundmass mostly composed of microlites of plagioclase, clinopyroxene, and Fe–Ti oxides, and

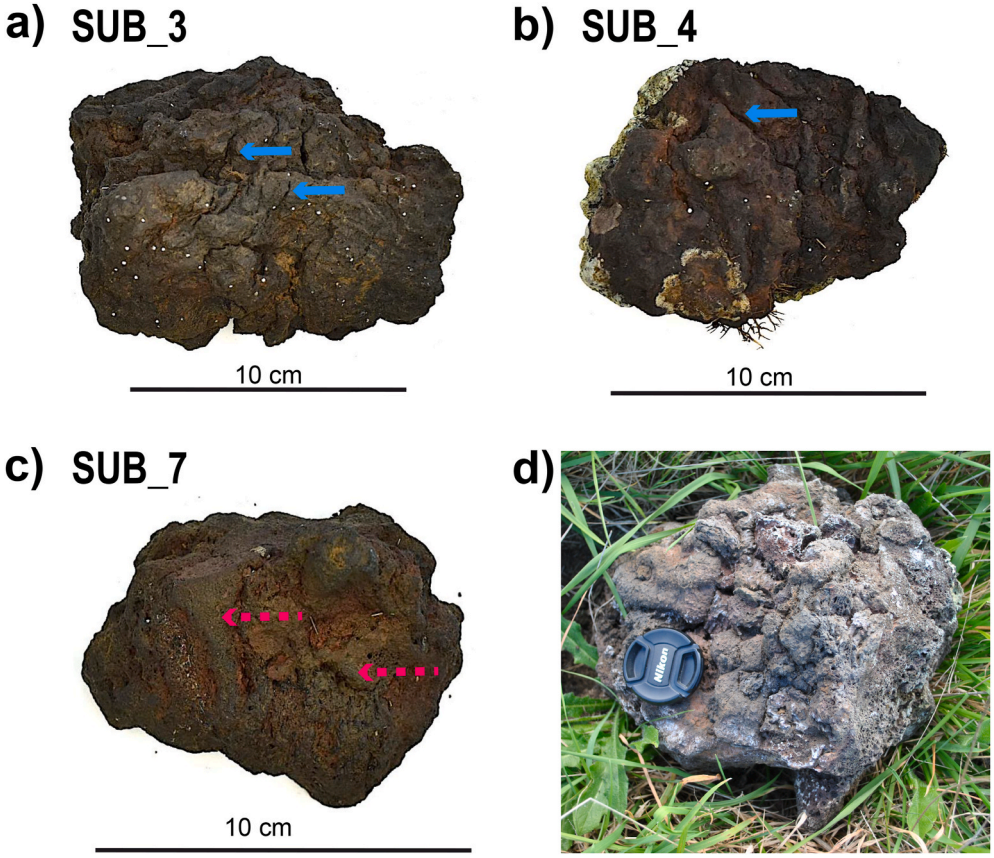

Fig. 3. Examples of hand-specimens collected at Stanley Patch volcano (a–c). Textural features such as cooling cracks (blue solid arrows) and deformation structures (red dashed arrows), are also indicated. d) Block fragment formed through subaerial lava fountaining activity in the Otuataua scoria cone (−36.985189°, 174.753150°) from the Quaternary Auckland Volcanic Field, New Zealand.

interstitial glass (Hopfenblatt, 2019). The vesicles are randomly distributed displaying collapsed and coalescent structures with vesicularity, ranging from c. 20 to 50 vol %. Vesicular patterns are typical to nucleation of a segregated gas phase within an ascending magma causing degassing and fragmentation at shallow depths (Valentine et al., 2005; Shea et al., 2010; Kereszturi and Nemeth, 2016). The samples show lack of palagonitization, quenched rims, and hyaloclastites, which are typical for underwater and emerging volcanoes, such as Surtsey Island near Iceland (e.g. Van Otterloo, 2015; Jackson et al., 2019). This suggests that the samples have not experienced excessive hydration, oxidation and zeolitization processes. The whole-rock geochemistry indicates that the Stanley Patch products are subalkaline basaltic andesites to basaltic trachyandesites (53–55 wt% SiO_2) falling within the compositional trend described by the Deception Island magmas (Fig. 4) (e.g., Aparicio 1997; Smellie 2002; Geyer et al., 2019).

Geochemistry of the sediments. The properties and composition of the sediment column are homogeneous and do not change substantially with depth (Fig. 5, Appendix B). Textural composition is clearly dominated by the sand fraction (66–77%), followed by the silt fraction (22–34%), and by clay in a very low proportion (generally <1%). The overall TOC is very low (generally <0.03%) and, consequently, TN and TS contents are also low (generally, TN <0.01% and TS < 0.05%). The ratio TOC/TN was always less than 20, indicating a marine origin of the organic matter (Emerson and Hedges, 1988).

Sediment reaction shows values close to neutral (pH = 6.6–7.3), and the grey color of the matrix (5Y3/2, Munsell Color Chart) suggest iron-reducing redox conditions (suboxic conditions), while the sparse reddish spots (2.5 YR 3/6) associated with bioturbation channels suggest the presence of oxic microsystems related to benthic faunal activity. Additionally, the presence of metastable iron sulphide forms at very low concentrations (acid volatile sulphides, AVS: 0.09–0.20 μmol g^{-1}) indicates the presence of anoxic microsystems in the sediment column, where organic matter is mineralized by sulphate-reducing bacteria (SRB). The low AVS and pyrite (FeS_2) contents indicate the absence of metal sulphides released by volcanic activity, as occurs in other oceanic hydrothermal environments (e.g. Otero et al., 2003).

Macrobenthic biodiversity. Most of the macrobenthic organisms observed during collection were vagile (Fig. 6). A total of 11 species (species richness) were identified, belonging to 5 phyla (Table 1). High densities of the two most common echinoderms of Deception Island were observed, the brittle star *Ophionotus victoriae* Bell, 1902, and the sea urchin *Sterechinus neumayeri* (Meissner, 1900), along with the bivalve mollusc *Laternula elliptica* (King, 1832). All of them showed a uniform distribution in the sampled area, whereas the sea star *Odontaster Validus* Koehler, 1906 and the nemertenean *Parborlasia corrugatus* (McIntosh, 1876) displayed medium abundances with patchy distributions. The abundances of the brittle stars and sea urchins range in hundreds of individuals (200-400 m^{-2}), while the abundance of bivalves are an order of magnitude less (50-80 m^{-2}). When occasional boulders were found, sessile filter and suspension feeders were present (Fig. 6), such as the demosponges *Dendrilla antarctica* Topsent, 1905, *Kirkpatrickia variolosa* (Kirkpatrick, 1907), *Hemigellius pilosus* (Kirkpatrick, 1907), and *Mycale (Oxymycale) acerata* Kirkpatrick, 1907, the tunicate *Cnemidocarpa verrucosa* (Lesson, 1830), and some smaller animals that live on these megabenthic organisms, such as annelid polychaetes (Terebellidae, Polynoidea), crustaceans (Isopoda and Amphipoda), and the nudibranch mollusc *Doris kerguelenensis* (Bergh, 1884).

4. Discussion

Stanley Patch volcanic cone presents many challenging features for interpreting its origin due to the semi-enclosed nature of Port Foster, the presence of hydrothermal activity, the variations in topography, and basin morphological features. The morphology and size of the Stanley Patch cone (e.g. Wcr/Wco and Hco/Wco) and the textural characteristics of the recovered pyroclastic rocks (e.g. vesicles volume and shape) indicate that this volcanic edifice was constructed during a monogenetic explosive volcanic eruption (e.g. Németh and Kereszturi, 2015). A monogenetic origin for Stanley Patch volcano is also in agreement with the rest of post-caldera volcanic features observed onshore on Deception

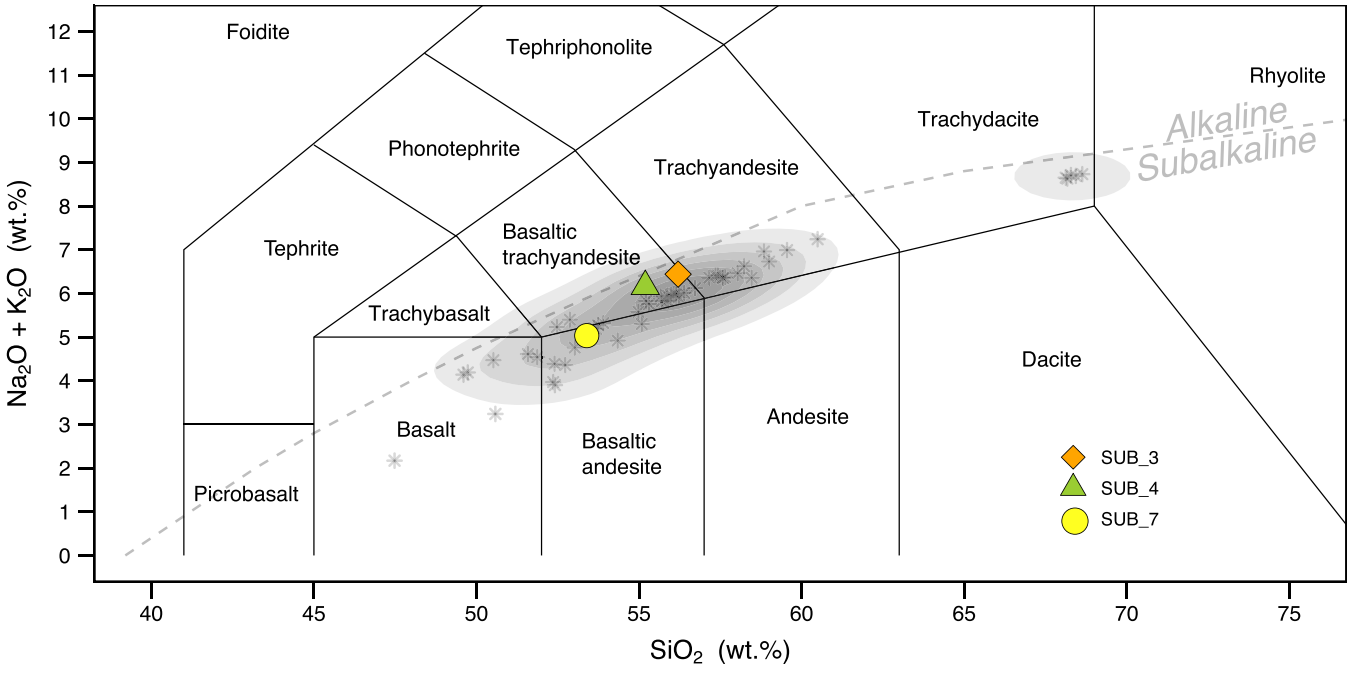

Fig. 4. Total alkalis versus silica diagram (TAS) (Le Bas et al., 1986) for the three geochemically analyzed Stanley Patch rock samples: SUB_3, SUB_4 and SUB_7 (see Appendix A for details on composition and latitude-longitude coordinates of the rock samples). For comparison grey shaded areas and asterisks correspond to the post-caldera rock samples presented by Geyer et al. (2019). Major elements normalized to 100% (anhydrous) with Fe distributed between FeO and Fe_2O_3 following Middlemost (1989). Grey dashed line discriminates between the alkaline-subalkaline fields (Irvine et al., 1971). See main text for more details.

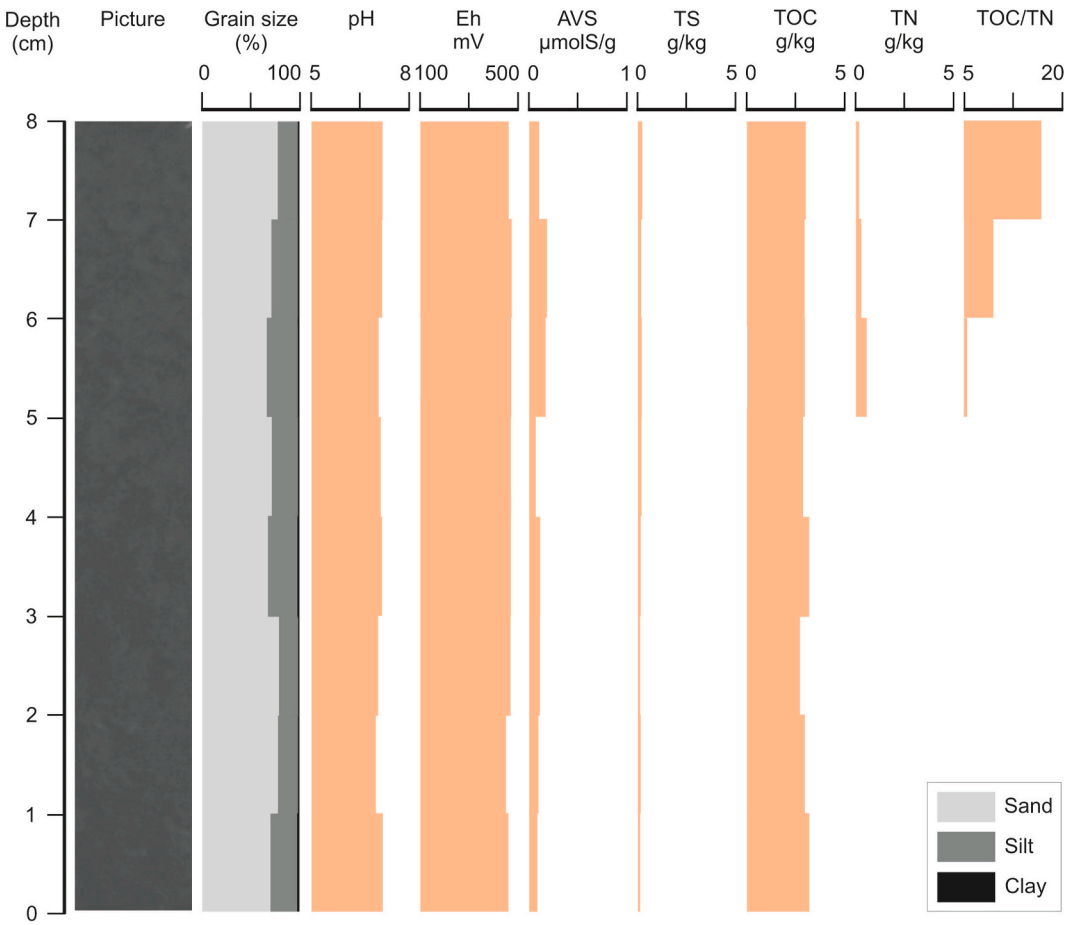

Fig. 5. Schematic log of the core, indicating sedimentological and geochemical characteristics. AVS: Acid volatile sulphide (FeS, Fe_3S_4); TS: total sulfur; TOC: total organic carbon; TN: total nitrogen; TOC/TN: ratio organic carbon to total N.

Island, such as tuff rings, tuff cones, and scoria cones (Bartolini et al., 2014; Pedrazzi et al., 2014, 2020). The Hco/Wco ratio of 0.13 is in line with both submarine (e.g. Cavallaro and Coltelli, 2019; Weiß et al., 2015) (Fig. 2d), and subaerial pyroclastic cones when: (1) the cone flank is immature, or (2) the cone has been partially eroded (Riedel et al., 2003; Kereszturi and Németh, 2012). The slope and major geometry of the flank are usually maintained due to the angle of repose of natural scoria that is 33° (e.g. Wood, 1980). This repose angle value yields a Hco/Wco ratio of 0.2. However, when there is limited scoria available, the growing cone never reaches 33° (e.g. McGetchin et al., 1974) thus maintaining the value of 0.2. This can explain the relatively small size and apparent low Hco/Wco ratio of Stanley Patch volcano. However, the Wcr/Wco ratio, and flank morphology are in the same range as for terrestrial scoria cones (e.g., Kervyn et al., 2012; Settle, 1979; Wood, 1980b) (Fig. 2e).

Additionally, the lack of palagonitization (i.e. significant alteration of the volcanic glass by water interaction) and quenched rims of the collected samples and apparent absence of hyaloclastites suggest that the explosive eruptions leading to the growth of Stanley Patch, must have taken place under "dry"-subaerial conditions, despite the common phreatic and phreatomagmatic activity described in the island (Pedrazzi et al., 2018; Álvarez-Valero et al., 2020). This may reveal changes of the sea level within Port Foster, subsidence processes of the caldera floor since the caldera-forming event until present day, and/or even that the caldera depression was enclosed for a certain time (Hopfenblatt, 2019).

Geochemical and petrologic analysis of the Stanley Patch rocks (e.g. fine-grained textures, similar geochemistry to the subaerial volcanoes) support a similar petrogenesis compared to the on-shore post-caldera volcanoes. Bulk rock geochemistry fits within the post-caldera magmatic trend (Smellie, 2002; Geyer et al., 2019). Geyer et al. (2019) revealed the existence of a complex plumbing system beneath Deception Island, composed of several shallow reservoirs (≤10 km depth) fed by magmas directly from the mantle, or from a magma accumulation zone located at the crust-mantle boundary (15–20 km). According to these authors, during the post-caldera stage, erupted magma can be either directly supplied by the reservoir located at the crust-mantle boundary or by magma batches located at different depths (at 10–11 km and <10 km). In the case of the Stanley Patch magmas whole-rock compositions suggest that the erupted material is compatible to magma reservoirs located at depths greater than 10 km (Geyer et al., 2019). Further detailed studies on geochemistry and petrology in the Stanley Patch rocks (stable isotopes, mineral chemistry, and pressure-temperature estimates) are necessary to precisely determine the origin and evolution of magma beneath Stanley Patch cone (Hopfenblatt, 2019).

Low TOC content in the sediments reflects the subpolar climatic conditions and the presence of sea-ice, due to its effects on primary productivity rates. On the other hand, several studies showed a decrease of TOC and an increase of mineral content in the coldest periods when there is a more extensive sea-ice coverage (Domack et al., 1995; Shevenell et al., 1996; Yoon et al., 2007). Moreover, organic degradation is less efficient at higher burial rates. Above a critical sedimentation rate, TOC typically decreases with increasing sedimentation rate owing to classic dilution of the organic input (Johnson, 1982). In Port Foster, sedimentation rates are high due to several factors: (1) fine volcanic sedimentary particles (e.g. ash and lapilli), and (2) melting of snow cover during the austral summer, causing run-off, with the presence of active gullies, alluvial fans, debris flows, and mudflows (Inbar, 1995; López-Martínez et al., 1999). In the volcanic eruptions of the 1960s and

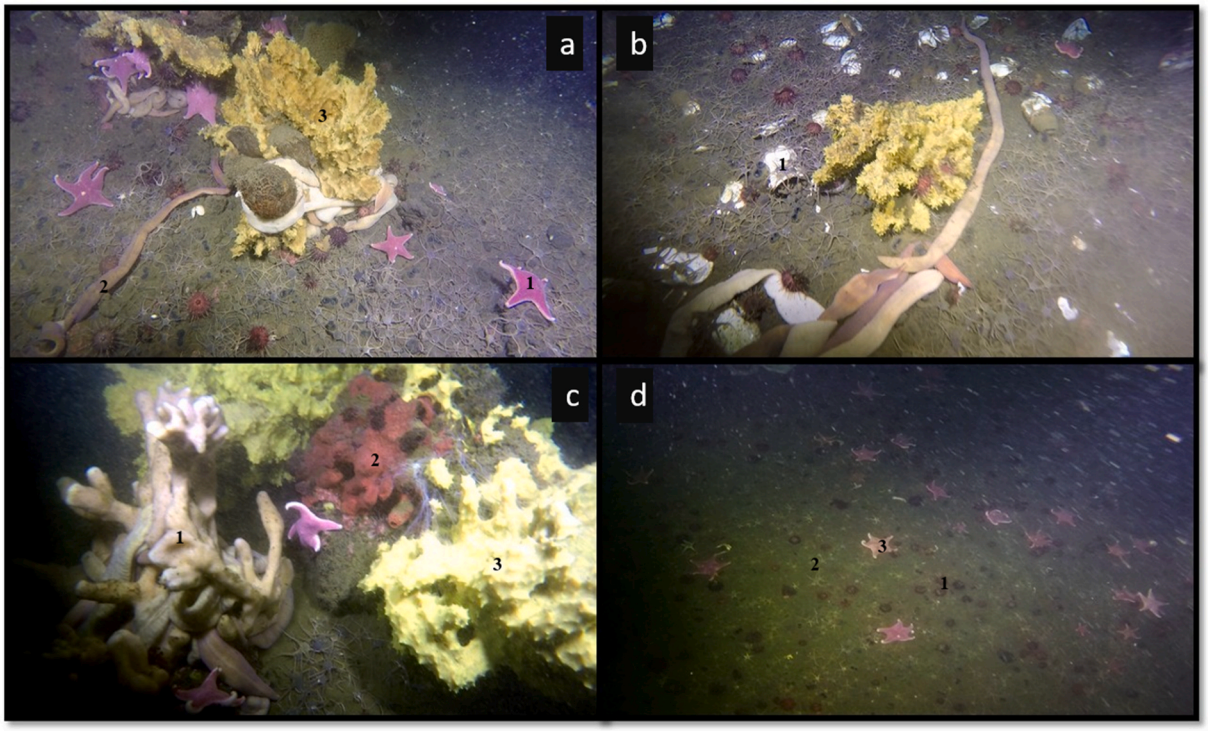

Fig. 6. Photographs taken by divers on the top of the crater. **(a)** The sea star *Odontaster validus* (1), the worm *Parborlasia corrugatus* (2), and the sponge *Dendrilla antarctica* (3). **(b)** *Dendrilla antarctica*, cluster of *P. corrugatus*, and shells of the mollusc *Laternula elliptica* (1). **(c)** The sponges *Hemigellius pillosus* (1), *Kirkpatrickia variolosa* (2), and *Dendrilla antarctica* (3). **(d)** High densities of the sea urchin *Sterechinus neumayeri* (1), the brittle star *Ophionotus victoriae* (2), and the sea star *Odontaster validus* (3).

Table 1
Species identified in the video transect, ordered by semi-quantitative abundances.

Phyllum	Class or Order	Taxa	Density	Abundance
Echinodermata	Ophiuroidea	*Ophionotus victoriae* Bell, 1902	high	200-500/m^2
Echinodermata	Echinoidea	*Sterechinus neumayeri* (Meissner, 1900)	high	100-200/m^2
Mollusca	Bivalvia	*Laternula elliptica* (P.P. King, 1832)	high	50-100/m^2
Echinodermata	Asteroidea	*Odontaster validus* Koehler, 1906	medium	10/m^2
Nemertean	Heteronemertea	*Parborlasia corrugatus* (McIntosh, 1876)	medium	10/m^2
Porifera	Demospongia	*Dendrilla antarctica* Topsent, 1905	low	<1/m^2
Porifera	Demospongia	*Mycale (Oxymycale) acerata* Kirkpatrick, 1907	low	<1/m^2
Porifera	Demospongia	*Hemigellius pilosus* (Kirkpatrick, 1907)	low	<1/m^2
Porifera	Demospongia	*Kirpatrickia variolosa* (Kirkpatrick, 1907)	low	<1/m^2
Mollusca	Gastropoda	*Doris kerguelenensis* (Bergh, 1884)	low	<1/m^2
Chordata	Ascidiacea	*Cnemidocarpa verrucosa* (Lesson, 1830)	low	<1/m^2

1970s, the formation of lahars and pyroclastic density currents has been observed in various areas of Deception Island (Bartolini et al., 2014). These events give rise to a rapid sediment flux. Moreover, the degradation of permafrost, increased by the geothermal activity of the volcano (Goyanes et al., 2014), also contributes to the mobilization of water and sediment.

Similarly, those glacial fronts reaching the coastal areas also play a key role in coastal erosion and sedimentation processes (Griffith and Anderson, 1989). In the studied sediment core, the reddish mottles and high Eh values (Eh > 400 mV) may be connected with oxic microsystems due to the high densities of infaunal organisms found in sediment cores of the shallow-water (5–15 m depth) of Deception Island (Angulo-Preckler et al., 2017a). Iron-reduction redox conditions (suboxic conditions) were also identified, yet low sulphate-reduction activity in these sediments could favor the flux of Fe to the water column. This process can be very important considering that iron is a key delimiting or co-limiting micronutrient for biological production in most oceans, including the Southern Ocean (Moore et al., 2009, 2013).

Port Foster receives a massive sediment discharge into the seawater through glacier activity, and surface wash combined with seismic tremors that drive remobilization of water-saturated sediments (Inbar, 1995). Although there are other sources of nutrients involved in productivity, the low organic content in the sediment reflects the subpolar climate and the present-day morphodynamics, related to volcanism and the glacial, periglacial and slope landforms and processes that affect the basin sedimentation. All these physical factors produce oxic microsystems (probably due to the high densities of infaunal organisms), and suboxic conditions that favor the flux of Fe to the water column.

The current benthic community was apparently established since the last eruptions that devastated all of the sea bottom community of Deception Island during 1967–1970 (Elderfield, 1972). This local devastation of the fauna is one of the most severe disturbances, especially because recovery in the Antarctic ecosystem is slow due to its low

productivity (Gutt et al., 1996). This recolonization process seems to be recurrent along the history of Deception Island since the caldera was flooded for the first time. Many taxa are poorly represented, and the colonizers are mainly opportunistic species with planktotrophic larvae (Barnes et al., 2008). In fact, it has been suggested that the modern benthic community has reached the highest level of organization that the temporal frequency of the volcanic activity of the island allows (Lovell and Trego, 2003; Angulo-Preckler et al., 2017a, 2018).

The extreme habitat conditions that characterize Antarctic ecosystems provide many opportunities to study how benthic species and communities respond to physical disturbance, underlining the importance of substratum stability as the structuring factor of the benthic communities in Deception Island. Punctuated disturbance (volcanic eruptions and degassing) and chronic disturbance (high sedimentation rates and sediment instability) seem to be the key fundamental factors that shape the macrobenthic communities at Deception Island. Concerning the former, there is evidence of direct relationships between volcanic emissions (e.g. gas) and organism reactions in other submarine volcanoes (Fraile-Nuez et al., 2012; Álvarez-Valero et al., 2018). Antarctic ecosystems are described to have great resilience, since they are subject to continuous physical impacts (Peck et al., 2009; Kapsenberg and Hofmann, 2014). Due to the strong instability of the soft sediment bottoms on Deception Island slopes (Inbar, 1995; Melo et al., 2012), the development of a sessile filter feeder community is difficult, thus favoring opportunistic detritivores (Angulo-Preckler et al., 2018). Furthermore, a community dominated by infauna, with surface and subsurface feeders, is related to a high biogenic sedimentation rate (Ravaioli et al., 1999). This opens the chance for well-developed epibenthic and infaunal communities (Angulo-Preckler et al., 2017a, 2017b). In addition, the high abundance of some predator species, such as *Odontaster validus* (sea star) and *Parborlasia corrugatus* (nemertean) requires high amounts of available food. This is reinforced by the important presence of dead shells of the bivalve *Laternula elliptica,* probably the main prey of these voracious predators. Typically, Antarctic community assemblages include huge densities of mainly opportunistic deposit feeders, with mobile deposit feeders dominated by echinoderms, and a very abundant infauna (Gutt, 2007; Angulo-Preckler et al., 2017a). Moreover, the high concentrations of suspended particulate matter, the poor availability of light, and the sediment instability could be the reasons for the absence of macroalgae on this volcano.

A positive correlation between hard-substrates and biodiversity of macrobenthic species has been described in Deception Island (Angulo-Preckler et al., 2018). Dropstones provide hard substrate, increasing habitat heterogeneity, and may function as island habitats surrounded by sand. A random distribution of dropstones on the seafloor creates an heterogeneous distribution of fragmented hard substrata, forming the already mentioned island habitats. High rates of burial disturbance would not allow for a high diversity of benthic organisms, yet the competition is less severe for those species capable of coping with sediment instability. Moreover, the abrasion caused by sand and gravel put in motion by the waves and on an inclined slope, hinders sessile organisms from becoming permanently established in the shallow sublittoral zone.

5. Concluding remarks

Stanley Patch cone built up during an explosive monogenetic volcanic event. The apparent absence of typical petrologic features of submarine volcanic eruption in the studied samples such as palagonitization, quenched rims, and hyaloclastites suggest that Stanley Patch formed under "dry"-subaerial conditions, and subsequently partially eroded. When Neptunes Bellows collapsed, a massive influx of seawater entered into Port Foster, opening up for the first time a new area for marine benthic colonization. The volcanic history of the island has probably avoided the development of a stable benthic community over time, similar to other Antarctic shallow communities. Moreover, the current geomorphological conditions still shape different benthic communities than in the surrounding coastal ecosystems. This volcanic cone, and even the entire Port Foster, is a unique and special natural laboratory for benchmarking the rates of reestablishment of benthic communities on a volcanological-influenced shallow marine environment, offering data of great relevance for future studies evaluating the effects of global change on the seabed communities in Antarctica.

Ethical statement

The research reported here has been conducted in an ethical and responsible manner, and complies with all relevant legislation. We have no potential conflict of interest.

Funding

This work was developed within the BLUEBIO (CTM 2016-78901-R), POSVOLDEC (CTM 2016-79617-P) (AEI/FEDER-UE), CRONOANTAR (CTM 2016-77878-P), and VOLCLIMA (CGL 2015-72629-EXP/AEI) projects funded by the Spanish Government, altogether with IHM (Navy Hydrographic Spanish Institute), and IEO (Spanish Oceanographic Institute) support. C. A-P has been funded by the fundacion Ramon Areces. A.G. is grateful for her Ramon y Cajal contract (RYC-2012-11024). A-V, A.G. and G.K. also thank the assistance of the VOLGASDEC project (PGC 2018-095693-B-I00) (AEI/FEDER-UE).

Author contribution

M.G-B. identified the submarine cone through the real time bathymetry and contributed to design the logistic plan for sampling the cone with C.A-P., C.A., G.K., and A.A-V. C.A-P., P.P., and C.A. sampled the submerged volcano by scuba-diving. G.K., A.A-V., J.H–H., and A.G. studied the hand-specimens and carried out the morphometric, volcanic, petrologic and geochemical analysis. J.R–F. sample macroanalysis of the sediment, and J. C.: laboratory work, C.G–H. and X.L.O.: performed the geochemical analysis. C.A. and C.A.-P. identified taxonomically the invertebrates, and C.A-P. studied the images and the video transect. All the authors contributed to write and review the manuscript.

Declaration of competing interest

The authors declare that they have no known competing financial interests or personal relationships that could have appeared to influence the work reported in this paper.

Acknowledgements

Special thanks are due to the staff of "*BAE Gabriel de Castilla*" and the crew of the scientific vessel "*BIO Hesperides*" for their logistic support during the diving and bathymetric operations. This is a contribution to the AntEco (State of the Antarctic Ecosystem) SCAR Programme and the SCAR Expert Group on Antarctic Volcanism - AntVolc. This study is dedicated to the memory of the C.F. Francisco Javier Montojo (DGAM) who sadly passed away during that Antarctic expedition.

Appendix A. List of collected rock samples (62.98°S, 60.63°W). IGSN: International Geosample Number

Sample name	IGSN	Sample description
SUB_1	IED1800SUB1	Scoria fragment
SUB_2	IED1800SUB2	Scoria fragment
SUB_3	IED1800SUB3	Scoria fragment
SUB_4	IED1800SUB4	Scoria fragment
SUB_5	IED1800SUB5	Scoria fragment
SUB_6	IED1800SUB6	Scoria fragment
SUB_7	IED1800SUB7	Scoria fragment
SUB_8	IED1800SUB8	Scoria fragment
SUB_9	IED1800SUB9	Scoria fragment
SUB_10	IED1800SUB10	Scoria fragment
SUB_11	IED1800SUB11	Scoria fragment
SUB_12	IED1800SUB12	Scoria fragment
SUB_13	IED1800SUB13	Scoria fragment
SUB_14	IED1800SUB14	Scoria fragment
SUB_15	IED1800SUB15	Scoria fragment
SUB_16	IED1800SUB16	Scoria fragment
SUB_17	IED1800SUB17	Scoria fragment
SUB_18	IED1800SUB18	Scoria fragment
SUB_19	IED1800SUB19	Scoria fragment
SUB_20	IED1800SUB20	Scoria fragment
SUB_21	IED1800SUB21	Scoria fragment

Appendix B. Sedimentological and geochemical characterization of the sedimentary column. The concentrations are expressed in terms of dry weight of sediment (dw)

Sample	Depth (cm)	pH	Eh mV	AVS µmolS/g	TS g/kg	TOC g/kg	TN g/kg	TOC/TN	Sand %	Silt %	Clay %	Sedimentary texture
1	0–1	7.37	452	0.1259	0.46	3.05	0.18	16.66	77.00	22.92	0.08	loamy sand
2	1–2	7.28	467	0.1963	0.39	2.97	0.31	9.45	70.44	29.47	0.09	loamy sand
3	2–3	6.87	461	0.1743	0.44	3	0.57	5.28	65.91	33.99	0.10	sandy loam
4	3–4	7.08	459	0.0736	0.43	2.91	< LD	–	70.48	29.43	0.09	loamy sand
5	4–5	7.22	461	0.1407	0.36	3.24	< LD	–	67.37	32.52	0.10	sandy loam
6	5–6	6.82	459	0.1379	0.33	2.75	< LD	–	77.56	22.36	0.08	loamy sand
7	6–7	6.57	436	0.1051	0.36	3.01	< LD	–	76.85	23.07	0.08	loamy sand
8	7–8	7.28	449	0.0931	0.31	3.24	< LD	–	70.56	29.33	0.11	loamy sand

AVS: Acid volatile sulphide (FeS, Fe_3S_4); TOC: total organic carbon; TN: total nitrogen, LD: limit of detection; TS: total sulfur, TOC/TN: ratio organic carbon to total N.

References

Álvarez-Valero, A.M., Burgess, R., Recio, C., de Matos, V., Sánchez-Guillamón, O., Gómez-Ballesteros, M., Recio, G., Fraile-Nuez, E., Sumino, H., Flores, J.A., Ban, M., Geyer, A., Bárcenas, M.A., Borrajo, J., Compaña, J.M., 2018. Noble gas signals in corals predict submarine volcanic eruptions. Chem. Geol. 480, 28–34.

Álvarez-Valero, A.M., Gisbert, G., Aulinas, M., Geyer, A., Kereszturi, G., Polo-Sánchez, A., Núñez-Guerrero, E., Sumino, H., Borrajo, J., 2020. δD and δ18O variations of the magmatic system beneath Deception Island volcano (Antarctica): implications for magma ascent and eruption forecasting. Chem. Geol. 542, 119595.

Angulo-Preckler, C., Leiva, C., Avila, C., Taboada, S., 2017a. Macroinvertebrate communities from the shallow soft-bottoms of Deception Island (Southern Ocean): a paradise for opportunists. Mar. Environ. Res. 127, 62–74.

Angulo-Preckler, C., Tuya, F., Avila, C., 2017b. Abundance and size patterns of echinoderms in coastal soft-bottoms at deception island (South Shetland islands, Antarctica). Continent. Shelf Res. 137, 131–141.

Angulo-Preckler, C., Figuerola, B., Núñez-Pons, L., Moles, J., Martín-Martín, R., Rull-Lluch, J., Gómez-Garreta, A., Avila, C., 2018. Macrobenthic patterns at the shallow marine waters in the caldera of the active volcano of Deception Island, Antarctica. Continent. Shelf Res. 157, 20–31.

Antoniades, D., Giralt, S., Geyer, A., Álvarez-Valero, A.M., Pla-Rabes, S., Granados, I., Liu, E.J., Toro, M., Smellie, J.L., Oliva, M., 2018. The timing and widespread effects of the largest Holocene volcanic eruption in Antarctica. Sci. Rep. 8, 1–11.

Aparicio, A., Menegatti, N., Petrinovic, I., Risso, C., Viramonte, J.G., 1997. El volcanismo de Isla decepción (Península Antártida). Bol. Geol. Min. 108, 19–42.

Baldwin, R.J., Smith Jr., K.L., 2003. Temporal dynamics of particulate matter fluxes and sediment community response in Port Foster, Deception Island, Antarctica. Deep Sea Res. Part II Top. Stud. Oceanogr. 50, 1707–1725.

Baker, P.E., McReath, I., 1971. 1970 volcanic eruption at deception island. Nat. Phys. Sci. (Lond.) 231, 5–9.

Baker, P.E., McReath, I., Harvey, M.R., Roobol, M.J., Davies, T.G., 1975. The geology of the south Shetland islands: V. In: Volcanic Evolution of Deception Island, vol. 78. British Antarctic Survey.

Barker, P.E., 1982. The Cenozoic subduction history of the Pacific margin of the Antarctic Peninsula: ridge crest–trench interactions. J. Geol. Soc. 139, 787–801.

Barnes, D.K.A., Linse, K., Enderlein, P., Smale, D., Fraser, K.P.P., Brown, M., 2008. Marine richness and gradients at deception island, Antarctica. Antarct. Sci. 20, 271–280.

Bartolini, S., Geyer, A., Martí, J., Pedrazzi, D., Aguirre-Díaz, G., 2014. Volcanic hazard on deception island (South Shetland islands, Antarctica). J. Volcanol. Geoth. Res. 285, 150–168.

Brož, P., Hauber, E., 2013. Hydrovolcanic tuff rings and cones as indicators for phreatomagmatic explosive eruptions on Mars. J. Geophys. Res.: Plan 118, 1656–1675.

Brierley, A.S., 1999. A comparison of Antarctic *euphausiids* sampled by net and from geothermally heated waters: insights into sampling bias. Polar Biol. 22, 109–114.

Cavallaro, D., Coltelli, M., 2019. The graham volcanic field offshore southwestern sicily (Italy) revealed by high-resolution seafloor mapping and ROV images. Front. Earth Sci. 7, 311.

Cline, J.D., 1969. Spectrophotometric determination of hydrogen sulfide in natural waters. Limnol. Oceanogr. 14, 454–458.

Cranmer, T.L., Ruhl, H.A., Baldwin, R.J., Kaufmann, R.S., 2003. Spatial and temporal variation in the abundance, distribution and population structure of epibenthic megafauna in Port Foster, Deception Island. Deep Sea Res. Part II Top. Stud. Oceanogr. 50, 1821–1842.

Dayton, P., Jarrell, S., Kim, S., Thrush, S., Hammerstrom, K., Slattery, M., Parnell, E., 2016. Surprising episodic recruitment and growth of Antarctic sponges: implications for ecological resilience. J. Exp. Mar. Biol. Ecol. 482, 38–55.

Dell, J.E., Salcido, D.M., Lumpkin, W., Richards, L.A., Pokswinski, S.M., Loudermilk, E.L., O'Brien, J.J., Dyer, L.A., 2019. Interaction diversity maintains resiliency in a frequently disturbed ecosystem. Frontiers in Ecology and Evolution 7, 145.

Domack, E.W., Ishman, S.E., Stein, A.B., McClennen, C.E., Jull, A.T., 1995. Late holocene advance of the müller ice shelf, antarctic Peninsula: sedimentological, geochemical and palaeontological evidence. Antarct. Sci. 7, 159–170.

Elderfield, H., 1972. Effects of volcanism on water chemistry, Deception Island, Antarctica. Mar. Geol. 13, 1–6.

Emerson, S., Hedges, J.I., 1988. Processes controlling the organic carbon content of open ocean sediments. Paleoceanography 3, 621–624. https://doi.org/10.1029/PA003i005p00621.
Favalli, M., Karátson, D., Mazzarini, F., Pareschi, M.T., Boschi, E., 2009. Morphometry of scoria cones located on a volcano flank: a case study from Mt. Etna (Italy), based on high-resolution LiDAR data. J. Volcanol. Geoth. Res. 186, 320–330.
Ferreira, T.O., Otero, X.L., Vidal-Torrado, P., Macias, F., 2006. Redox processes in mangrove soils under *Rhizophora mangle* in relation to different environmental conditions. Soil Sci. Soc. Am. J. 71, 484–491.
Fraile-Nuez, E., González-Dávila, M., Santana-Casiano, J.M., Arístegui, J., Alonso-González, I.J., Hernández-León, S., Blanco, M.J., Rodríguez-Santana, A., Hernández-Guerra, A., Gelado-Caballero, M.D., Eugenio, F., 2012. The submarine volcano eruption at the island of El Hierro: physical-chemical perturbation and biological response. Sci. Rep. 2, 486.
Gallardo, V.A., Castillo, J.G., 1968. Mass Mortality in the Benthic Infauna of Port Foster Resulting from the Eruptions in Deception Island. South Shetland Is.
Gallardo, V.A., Castillo, J.G., Retamal, M.A., Yanez, A., Moyano, H.I., Hermosilla, J.G., 1977. Quantitative Studies on the Soft-Bottom Macrobenthic Animal Communities of Shallow Antarctic Bays. Adaptations within Antarctic Ecosystems. Smithsonian Institution, Washington, DC, p. 361387.
Gee, G.W., Bauder, J.W., 1986. Particle-size analysis. In: Klute, A. (Ed.), Methods of Soil Analysis. Part 1. Physical and Mineralogical Methods. Soil Science Society of America, Madison, WI, USA, pp. 383–411.
Geyer, A., Álvarez-Valero, A.M., Gisbert, G., Aulinas, M., Hernández-Barreña, D., Lobo, A., Marti, J., 2019. Deciphering the evolution of Deception Island's magmatic system. Sci. Rep. 9, 373.
Goyanes, G., Vieira, G., Caselli, A., Cardoso, M., Marmy, A., Santos, F., Bernardo, I., Hauck, C., 2014. Local influences of geothermal anomalies on permafrost distribution in an active volcanic island (Deception Island, Antarctica). Geomorphology 225, 57–68.
Griffith, T.W., Anderson, J.B., 1989. Climatic control of sedimentation in bays and fjords of the northern Antarctic Peninsula. Mar. Geol. 85, 181–204.
Gutt, J., Starmans, A., Dieckmann, G., 1996. Impact of iceberg scouring on polar benthic habitats. Mar. Ecol. Prog. Ser. 137, 311–316.
Gutt, J., 2007. Antarctic macro-zoobenthic communities: a review and an ecological classification. Antarct. Sci. 19, 165–182.
Hopfenblatt, J., 2019. Characterisation of the submarine cone Stanley Patch, deception island (Antarctica): implications for volcanic hazard assessments. Master Thesis. University of Barcelona.
Huerta-Diaz, M.A., Morse, J.W., 1992. Pyritization of trace metals in anoxic marine sediments. Geochem. Cosmochim. Acta 56, 2681–2702.
Inbar, M., 1995. Fluvial morphology and streamflow on deception island, Antarctica. Geogr. Ann. Phys. Geogr. 77, 221–230.
Irvine, T.N., Baragar, W.R.A., 1971. A guide to the chemical classification of the common volcanic rocks. Can. J. Earth Sci. 8, 523–548.
Jackson, M.D., Couper, S., Stan, C.V., Ivarsson, M., Czabaj, M.W., Tamura, N., Parkinson, D., Miyagi, L.M., Moore, J.G., 2019. Authigenic mineral texture in submarine 1979 basalt drill core, Surtsey volcano, Iceland. G-cubed 20, 3751–3773.
Johnson, L.E., 1982. Relationship between sedimentation rate and total organic carbon content in ancient marine sediments. AAPG (Am. Assoc. Pet. Geol.) Bull. 66, 170–188.
Kapsenberg, L., Hofmann, G.E., 2014. Signals of resilience to ocean change: high thermal tolerance of early stage Antarctic sea urchins (*Sterechinus neumayeri*) reared under present-day and future pCO_2 and temperature. Polar Biol. 37, 967–980.
Kereszturi, G., Németh, K., 2012. Monogenetic basaltic volcanoes: genetic classification, growth, geomorphology and degradation. In: Németh, K. (Ed.), Updates in Volcanology - New Advances in Understanding Volcanic Systems, pp. 3–88.
Kereszturi, G., Németh, K., 2016. Sedimentology, eruptive mechanism and facies architecture of basaltic scoria cones from the Auckland Volcanic Field (New Zealand). J. Volcanol. Geoth. Res. 324, 41–56.
Kervyn, M., Ernst, G.G.J., Carracedo, J.C., Jacobs, P., 2012. Geomorphometric variability of "monogenetic" volcanic cones: evidence from Mauna Kea, Lanzarote and experimental cones. Geomorphology 136, 59–75.
Kostka, J.E., Luther III, G.W., 1994. Partitioning and speciation of solid phase iron in saltmarsh sediments. Geochem. Cosmochim. Acta 58, 1701e1710.
Le Bas, M.J., Le Maitre, R.W., Streckeisen, A., Zanettin, B.A., 1986. Chemical classification of volcanic rocks based on the total Alkali-silica diagram. J. Petrol. 27, 745–750.
LeMasurier, W.E., Thomson, J.W., 1990. Volcanoes of the antarctic plate and southern oceans. Antarct. Res. 48 (71), 799.
López-Martínez, J., Serrano, E., Rey, J., Smellie, J.L., 1999. Geomorphological Map of Deception Island. E. 1/25000. BAS Geomap Series, 7B. British Antarctic Survey, Cambridge.
Lovell, L.L., Trego, K.D., 2003. The epibenthic megafaunal and benthic infaunal invertebrates of Port foster, deception island (South Shetland islands, Antarctica). Deep Sea Res. Part II Top. Stud. Oceanogr. 50, 1799–1819.
Martí, J., Geyer, A., Aguirre-Diaz, G., 2013. Origin and evolution of the deception island caldera (South Shetland islands, Antarctica). Bull. Volcanol. 75, 732.
Martos, Y.M., Catalán, M., Galindo-Zaldívar, J., Maldonado, A., Bohoyo, F., 2014. Insights about the structure and evolution of the Scotia Arc from a new magnetic data compilation. Global Planet. Change 123, 239–248.
McGetchin, T.R., Settle, M., Chouet, B.A., 1974. Cinder cone growth modeled after northeast Crater, Mount Etna, Sicily. J. Geophys. Res. 79, 3257–3272.
Melo, R., Vieira, G., Caselli, A., Ramos, M., 2012. Susceptibility modelling of hummocky terrain distribution using the information value method (Deception Island, Antarctic Peninsula). Geomorphology 155–156, 88–95.
Middlemost, E.A.K., 1989. Iron oxidation ratios, norms and the classification of volcanic rocks. Chem. Geol. 77, 19–26.
Mitchell, N.C., Stretch, R., Oppenheimer, C., Kay, D., Beier, C., 2012. Cone morphologies associated with shallow marine eruptions: east Pico Island, Azores. Bull. Volcanol. 74, 2289–2301.
Monien, D., Monien, P., Brünjes, R., Widmer, T., Kappenberg, A., Busso, A.A.S., Schnetger, B., Brumsack, H.J., 2017. Meltwater as a source of potentially bioavailable iron to Antarctica waters. Antarct. Sci. 29, 277–291.
Moore, C.M., Mills, M.M., Achterberg, E.P., Geider, R.J., LaRoche, J., Lucas, M.I., McDonagh, E.L., Pan, X., Poulton, A.J., Rijkenberg, M.J., Suggett, D.J., 2009. Large-scale distribution of Atlantic nitrogen fixation controlled by iron availability. Nat. Geosci. 2, 867–871.
Moore, C.M., Mills, M.M., Arrigo, K.R., Berman-Frank, I., Bopp, L., Boyd, P.W., Galbraith, E.D., Geider, R.J., Guieu, C., Jaccard, S.L., Jickells, T.D., 2013. Processes and patterns of oceanic nutrient limitation. Nat. Geosci. 6, 701–710.
Németh, K., Kereszturi, G., 2015. Monogenetic volcanism: personal views and discussion. Int. J. Earth Sci. 104, 2131–2146.
Orheim, O., 1972. A 200-year Record of Glacier Mass Balance at Deception Island, Southwest Atlantic Ocean, and its Bearing on Models of Global Climate Change. Institute of Polar Studies, Ohio State University.
Otero, X.L., Huerta-Díaz, M.A., Macias, F., 2003. Influence of a turbidite deposit on the extent of pyritization of iron, manganese and trace metals in sediments from the Guaymas Basin, Gulf of California (Mexico). Appl. Geochem. 18, 1149–1163.
Pasotti, F., Manini, E., Giovannelli, D., Wölfl, A.C., Monien, D., Verleyen, E., Braeckman, U., Abele, D., Vanreusel, A., 2015. Antarctic shallow water benthos in an area of recent rapid glacier retreat. Mar. Ecol. 36, 716–733.
Peck, L.S., Clark, M.S., Morley, S.A., Massey, A., Rossetti, H., 2009. Animal temperature limits and ecological relevance: effects of size, activity and rates of change. Funct. Ecol. 23, 248–256.
Pedrazzi, D., Aguirre-Díaz, G., Bartolini, S., Martí, J., Geyer, A., 2014. The 1970 eruption on Deception Island (Antarctica): eruptive dynamics and implications for volcanic hazards. J. Geol. Soc. 171, 765–778.
Pedrazzi, D., Németh, K., Geyer, A., Álvarez-Valero, A.M., Aguirre-Díaz, G., Bartolini, S., 2018. Historic hydrovolcanism at Deception Island (Antarctica): implications for eruption hazards. Bull. Volcanol. 80, 11.
Pedrazzi, D., Kereszturi, G., Lobo, A., Geyer, A., Calle, J., 2020. Geomorphology of the post-caldera monogenetic volcanoes at Deception Island, Antarctica. Implications for landform recognition and volcanic hazard assessment. J. Volcanol. Geoth. Res. 402, 106986.
Pickett, S.T., Kolasa, J., 1991. Ecological Heterogeneity. Springer-Verlag.
Ponnamperuma, F.N., 1972. The chemistry of submerged soils. In: Advances in Agronomy, vol. 24. Academic Press, pp. 29–96.
Ravaioli, M., Frignani, M., Gambi, M.C., Labbrozzi, L., Langone, L., 1999. Particle fluxes and sediment characteristics at three selected sites in the Ross Sea (Antarctica). In: Oceanography of the Ross Sea Antarctica. Springer, Milano, pp. 209–222.
Rey, J., Somoza, L., Hernandez-Molina, F.J., 1992. Formas de los sedimentos submarinos superficiales en Puerto Foster, Isla Decepción, Islas Shetland del Sur.
Rey, J., Somoza, L., Martínez-Frías, J., 1995. Tectonic, volcanic, and hydrothermal event sequence on Deception Island (Antarctica). Geo Mar. Lett. 15, 1–8.
Riedel, C., Ernst, G.G.J., Riley, M., 2003. Controls on the growth and geometry of pyroclastic constructs. J. Volcanol. Geoth. Res. 127, 121–152.
Robinson, B.J., Barnes, D.K., Morley, S.A., 2020. Disturbance, dispersal and marine assemblage structure: a case study from the nearshore Southern Ocean. Mar. Environ. Res. 105025.
Roobol, M.J., 1973. Historic volcanic activity at deception island. Br. Antarct. Surv. Bull. 32, 23–30.
Roobol, M.J., 1980. A model for the eruptive mechanism of Deception Island from 1820 to 1970. Br. Antarct. Surv. Bull. 49, 137–156.
Roobol, M.J., 1982. The volcanic hazard at deception island, South Shetland islands. Br. Antarct. Surv. Bull. 51, 237–245.
Settle, M., 1979. The structure and emplacement of cinder cone fields. Am. J. Sci. 279, 1089–1107.
Shea, T., Houghton, B.F., Gurioli, L., Cashman, K.V., Hammer, J.E., Hobden, B.J., 2010. Textural studies of vesicles in volcanic rocks: an integrated methodology. J. Volcanol. Geoth. Res. 190, 271–289.
Shevenell, A.E., Domack, E.W., Kernan, G.M., 1996. Record of Holocene palaeoclimate change along the Antarctic Peninsula: evidence from glacial marine sediments, Lallemand Fjord. Pap. Proc. R. Soc. Tasman. 130, 55–64.
Smale, D., 2008. Spatial variability in the distribution of dominant shallow-water benthos at Adelaide Island, Antarctica. J. Exp. Mar. Biol. Ecol. 357, 140–148.
Smellie, J.L., López-Martínez, J., Headland, R.K., Hernández-Cifuentes, F., Maestro, A., Millar, I.L., Rey, J., Serrano, E., Somoza, L., Thomson, J.W., 2002. Geology and geomorphology of deception island. British Antarctic Survey.
Smellie, J.L., 2002. Geology. In: López-Martínez, J., Smellie, J.L., Thomson, J.W., Thomson, M.R.A. (Eds.), Geology and Geomorphology of Deception Island. British Antarctic Survey, Cambridge, BAS GEOMAP Series, Sheets 6-A and 6-B, 1:25 000, Cambridge, pp. 11–30.
Somoza, L., Martınez-Frıas, J., Smellie, J.L., Rey, J., Maestro, A., 2004. Evidence for hydrothermal venting and sediment volcanism discharged after recent short-lived volcanic eruptions at Deception Island, Bransfield Strait, Antarctica. Mar. Geol. 203, 119–140.
Torrecillas, C., Berrocoso, M., García-García, A., 2006. The multidisciplinary scientific information support system (SIMAC) for deception island. Antarctica Springer, Berlin, Heidelberg, pp. 397–402.
Valentine, G.A., Krier, D., Perry, F.V., Heiken, G., 2005. Scoria cone construction mechanisms. Lathrop Wells volcano, southern Nevada, USA. Geology 33, 629–632.

Van Otterloo, J., Cas, R.A.F., Scutter, C.R., 2015. The fracture behaviour of volcanic glass and relevance to quench fragmentation during formation of hyaloclastite and phreatomagmatism. Earth Sci. Rev. 151, 79–116.
Weiß, B.J., Hübscher, C., Wolf, D., Lüdmann, T., 2015. Submarine explosive volcanism in the southeastern Terceira Rift/são Miguel region (Azores). J. Volcanol. Geoth. Res. 303, 79–91.
Wood, C.A., 1980. Morphometric evolution of cinder cones. J. Volcanol. Geoth. Res. 7, 387–413.
Wood, C.A., 1980b. Morphometric analysis of cinder cone degradation. J. Volcanol. Geoth. Res. 8, 137–160.
Yoon, H.I., Khim, B.K., Yoo, K.C., Bak, Y.S., Lee, J.I., 2007. Late glacial to Holocene climatic and oceanographic record of sediment facies from the South Scotia Sea off the northern Antarctic Peninsula. Deep Sea Res. Part II Top. Stud. Oceanogr. 54, 2367–2387.